Advanced Composite Materials
Publication details, including instructions for authors and subscription information:
http://www.tandfonline.com/loi/tacm20

Axial and lateral crushing of the filament wound laminated composite curved compound system

E. Mahdi , A. M. S. Hamouda & B. B. Sahari

Version of record first published: 02 Apr 2012.

To cite this article: E. Mahdi , A. M. S. Hamouda & B. B. Sahari (2002): Axial and lateral crushing of the filament wound laminated composite curved compound system , Advanced Composite Materials, 11:2, 171-192

To link to this article: http://dx.doi.org/10.1163/156855102760410351

Adv. Composite Mater., Vol. 11, No. 2, pp. 171–192 (2002)

Also available online - www.vsppub.com

Axial and lateral crushing of the filament wound laminated composite curved compound system

E. MAHDI [1,*], A. M. S. HAMOUDA [2] and B. B. SAHARI [2]

[1] *Aerospace Engineering Department, University Putra Malaysia, 43400 UPM, Serdang, Selangor, Malaysia*

[2] *Mechanical and Manufacturing Engineering Department, University Putra Malaysia, 43400 UPM, Serdang, Selangor, Malaysia*

Received 28 December 2001; accepted 17 April 2002

Abstract—In this paper, experimental and numerical investigations into the crushing behaviour of the filament wound laminated curved compound system have been conducted. The structure being investigated is composed of a complete and semi-circular cone-cylinder-cone system. The conical parts of the structure were symmetric. The cone vertex angle and the cylindrical part height were 15 degrees and 10 mm, respectively. Load–displacement curves and deformation histories of typical specimens are presented and discussed. The experimental data are correlated with predictions from finite element model. Numerical results show that for curved systems under lateral load, local stress has been concentrated at the junctions between the cylinder and cones as well as the edge of the systems, while for the curved systems under axial load, the stress concentration is slightly clear at the loaded end of the curved systems. Experimental results show that the axial loaded curved systems are crushed into a progressive failure mode and exhibit high-energy absorption capability. Results also show that the debonding at the fibre–matrix interface is influenced by the load–displacement relationship for the lateral loaded curved systems. On the other hand, the fragmentation failure mode is dominated by the load–displacement relationship for the axial loaded curved systems.

Keywords: Curved composite compound system; crushing behaviour; crashworthiness; finite element method.

NOMENCLATURE

E_s	Crushing energy absorbed per unit mass
E_v	Crushing energy absorbed per unit volume
P_m	Average crush load
P_i	Initial crush load
L	Maximum displacement
S	Instantaneous displacement

*E-mail: elsadig@eng.upm.edu.my

A	Cross-section area
M	Weight of the structure
C	Height of conical part
T	Height of cylindrical part
H	Total height of the structure
β	Semi-vertex angle of the cone
CFE	Crush force efficiency
SE	Stroke efficiency
D_2, D_1	Maximum and minimum diameters of the cone, respectively
FWL	Filament wound laminated
ACSEM	Axial crushing of FWL semi-circular curved compound systems
ACCOM	Axial crushing of FWL complete circular curved compound systems
LCSEM	Lateral crushing of FWL semi-circular curved compound systems
LCCOM	Lateral crushing of FWL complete circular curved compound system

1. INRODUCTION

During the last century, implementation of advanced materials in the design of energy absorber devices has been hampered by a lack of experimental and numerical simulation work that could guide the design of optimum energy absorber devices. So far, most of the available crashworthiness information that has been obtained relates to metal and composite single systems such as tubes, cones, etc. [1–9]. Whatever information exists for compound systems relates mostly to geometries untypical of crashworthiness devices, such as energy absorber devices [16–18]. However, energy absorber devices should satisfy two requirements — low weight and high crashworthiness. Based on energy data that has been generated to ensure the crashworthiness performance of composite materials based energy absorber devices, composite materials could significantly improve the safety performance of any vehicle type [10–15]. Consequently, composite materials are increasingly being exploited in automotive parts such as body panels, hoods and bumpers of automobiles. In the absence of full understanding of FWL curved compound system responses to different load conditions, designers usually resort to energy absorption generated data from responses of a composite single system, which could lead to conservative estimation. Most of the studies to examine the energy absorption capabilities of composite materials have been directed towards the axial crushing analysis of a composite single system, while in aerospace, automotive and marine applications it is often laminated curved compound systems that are subjected to impact damage. Therefore, the problem of investigating the response of a composite compound system subjected to different loading conditions should occupy considerable attention of scientists and designers in coming decades. Recently there have been a number of articles on aspects of the responses of a composite compound system to quasi-axial static compressive load. Papers have investigated the quasi-axial static crushing behaviour of different types of

composite compound system, including cone-cone and cone-tube-cone systems made of glass/epoxy and carbon/epoxy [19, 20].

The motivation of the present work is to explore the crashworthiness performance of FWL complete and semi-circular curved compound systems in terms of energy absorption to weight and volume ratios under different load conditions applied independently. The crush process was also modelled using the finite element method and fracture mechanics concepts combined with failure criteria developed for composite materials. The numerical model has been validated by comparison with experimental results.

2. CRASHWORTHINESS PARAMETERS

Motor vehicle accidents are due to human and environmental factors. Automobile manufacturers, by employing proper safety design and manufacturing techniques, can prevent many of the deaths and serious injuries that result from motor vehicle accidents. Accordingly, one of these techniques is to design and instal an energy absorber device, to prevent the vehicle's occupants from the effects of sudden impact [21]. They do this by converting the impact energy into plastic deformation energy in the case of metal car bodies and into fracture deformation in the case of composite materials car bodies, keeping the peak force exerted on the protected occupants below their tolerance level, which causes damage. They must also provide a long deformation path to sufficiently and gradually reduce the deceleration of the protected occupants [22, 23]. When evaluating the crashworthiness of an energy absorber device, great attention should be directed to its instantaneous crush force efficiency (*CFE*), the stroke efficiency (*SE*) and energy absorption capabilities.

2.1. Crush force efficiency (CFE)

The wide exploitation of advanced composites in energy absorber designs will depend to a large degree on the ability to support loads (average crush loads) well beyond the initial failure stage, which minimize second impact (occupant into vehicle interior) forces. This could be well demonstrated by evaluating the crush force efficiency (*CFE*), which can be calculated as

$$CFE = \frac{P_{\mathrm{m}}}{P_{\mathrm{i}}}, \tag{1}$$

where P_{i} and P_{m} represent initial and mean crush load, respectively. The latter can be obtained by averaging the crush load values over the crush displacements through the post-crush stage, while the former can be directly obtained from the load–displacement curve as the peak load value at initial failure crush stage. For an optimum crash unit, the CFE should be equal to one.

2.2. Stroke efficiency (SE)

As mentioned earlier, the desired energy absorber device should be crushable, in order to provide a long deformation path and gradual deceleration for the vehicle's

occupants. This can be demonstrated by calculating stroke efficiency of the energy absorber device as

$$SE = \frac{u}{H}, \tag{2}$$

where u and H represent the stroke and the total height of the structure, respectively.

2.3. Energy absorption

Two types of energy absorption during axial and lateral crushing of FWL complete and semicircular curved compound systems were measured. These are the energy absorbed per unit mass (E_s) and energy absorbed per unit volume (E_v). The former represents total work done (W_T), which is equal to the area under the load–displacement curve:

$$W_T = \int_{s_i}^{s} P \, ds. \tag{3}$$

The post-crush stage is generally more important due to its strong influence on the crashworthiness parameters. Therefore, work done at post-crush stage (W_P) can be calculated as

$$W_p = \int_{s_p}^{s} P_m \, ds \Rightarrow P_m(s - s_p). \tag{4}$$

Energy absorbed per unit mass (i.e. specific energy absorption) is given by

$$E_s = \frac{W_p}{M}. \tag{5}$$

By substituting equation (5) into equation (4)

$$E_s = \frac{P_m(s - s_p)}{\rho \times V_i} = \frac{P_m\left(\frac{s}{L} - \frac{s_p}{L}\right)}{\rho \times A} = \frac{P_m(SE - SE_p)}{\rho \times A}. \tag{6}$$

For complete crushing i.e. $s = L$, equation (6) can be re-written as

$$E_{s(s=L)} = \frac{P_m(s - s_p)}{\rho \times V_i} = \frac{P_m\left(\frac{s}{L} - \frac{s_p}{L}\right)}{\rho \times A} = \frac{P_m(1 - SE_p)}{\rho \times A}. \tag{7}$$

As stated earlier, the specific energy is not the only crucial design factor for energy absorber device crashworthiness performance; the energy absorbed per unit volume is also critical, where the space is a restraint. The volume occupied by the FWL complete compound system before crushing (i.e. at preloading state) can be

calculated as

$$V_i = V_{tube} + 2V_{cone} = \frac{\pi}{4} \times D_1^2 \times T + 2 \times \frac{\pi}{3}\left[D_2^2 \times C + \frac{D_1}{\tan\beta}\left[D_2^2 - D_1^2\right]\right]. \quad (8)$$

The energy absorbed per unit volume E_v can be calculated using equations (3) and (7) as

$$E_v = \frac{P_{m(s-s_p)}}{V_i} = \frac{P_m\left(\frac{s}{L} - \frac{s_p}{L}\right)}{V_i} = \frac{P_m(SE - SE_p)}{A}. \quad (9)$$

3. DESIGN PARAMETERS

Two design parameters have been used to explore and study the crashworthiness performance of FWL curved compound systems. These are the effects of loading condition and the geometry configuration. For the former, lateral and axial loads have been applied independently to the FWL composite curved compound systems. On the other hand, the latter includes two types of geometries: the FWL complete circular and the semi-circular curved compound systems.

4. EXPERIMENTAL PROGRAM

The structure being investigated is FWL complete and semi-curved compound systems made of glass/epoxy. All the specimens were 160 mm high (H), 70 mm minimum diameters of the cone (D_1) and 3 mm wall thickness as shown in Fig. 1. The mechanical properties of glass/epoxy are E_{11} = 38.4 GPa, E_{22} = 14.2

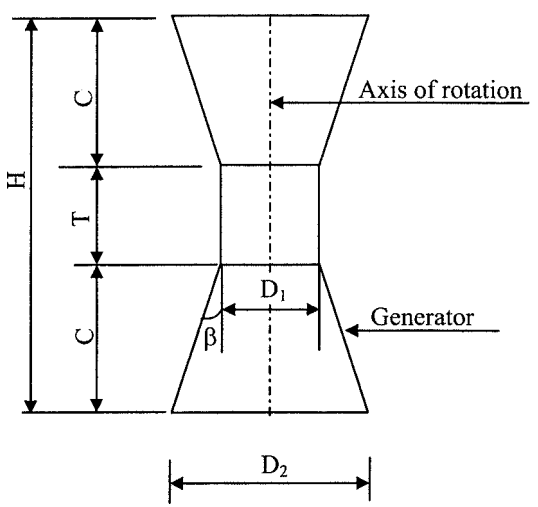

Figure 1. Notation used for FWL complete and semi-circular curved compound systems.

GPa, $G_{12} = G_{13} = 3.82$ GPa, $G_{23} = 3.22$ GPa, $\nu_{12} = \nu_{13} = 0.254$, $\nu_{23} = 0.458$. The stacking sequence of the FWL composite curved compound systems [24] was $[(90)_3/(55/-55)_2]_s$. A comprehensive compression test program has been performed on the FWL complete and semi-circular curved compound system specimens. A total of 12 specimens of the FWL complete and semi-curved compound systems were tested in axial and lateral compression. The cylindrical part height of the FWL compound system was 10 mm. Quasi-axial and lateral static crushing tests were carried out using an Instron 8500 digital-testing machine with full-scale load range of 250 kN. The compound system specimens were compressed between parallel, flat steel platens, one stagnant and one moving at an average strain rate of 2.5×10^{-4} s^{-1}. Load–displacement curves were recorded by an automatic data acquisition system. Three tests were performed for each specimen.

5. FINITE ELEMENT SIMULATION

In line with the experimental work, numerical simulation was also carried out. The finite element simulation was designed to predict the load–displacement curves, deformation histories and stresses throughout the FWL complete and semi-circular curved compound systems.

5.1. Model development

Detailed three-dimensional finite element models of the FWL complete and semi-circular curved compound systems was developed using the LUSAS finite element package. Typical meshes generated, shown in Fig. 2, consist of 11198 nodes, 3840 elements and 5599 nodes, 1920 elements for complete and serni-circular curved compound systems, respectively. An eight-noded (QTS8) element was used since this is expected to give accurate stress and strain results. This type of element also includes transverse shear effects. Hence, QTS8 was chosen for modelling the FWL curved compound system, for static non-linear analysis prediction. Each node has six degrees of freedom, which include three displacements, u_x, u_y, u_z and three rotation components, ϕ_x, ϕ_y and ϕ_z. With transverse shear effects, this element is expected to be more accurate compared with the stress element.

The laminate was modelled by defining each lamina with material properties, thickness, and fibre orientation. Fixing degrees of freedom at one end of the model in the x and y directions and applying the load at the other end by using a prescribed displacement simulated the testing conditions. Numerical simulation for the specimens is run until complete failure crush load is reached.

5.2. Failure model

To investigate the failure modes of filament wound laminated complete and semi-circular curved composite compound system, the Hill failure criterion is applied

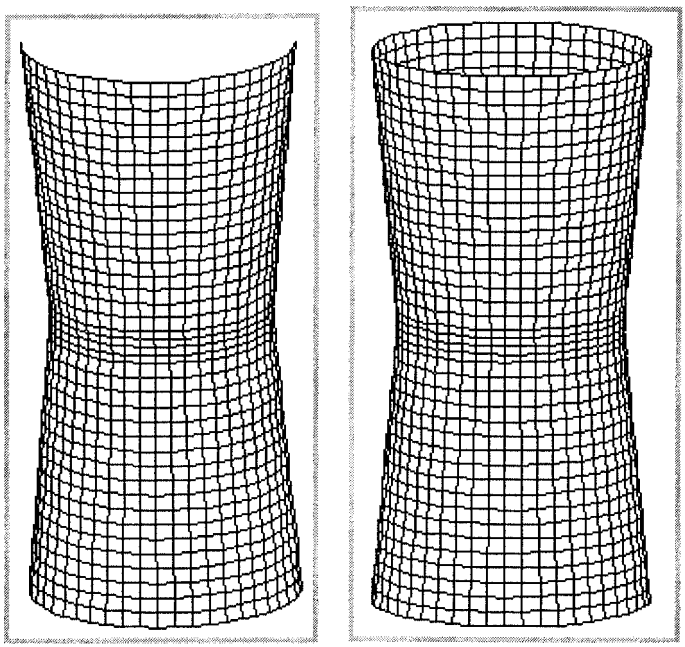

Figure 2. Typical mesh generation of FWL complete and semi-circular curved compound systems.

to the average stresses in the material direction of each element, because the failure modes can be predicted [25]. Therefore, by inputting yield stresses in each component direction, which are equal in tension and compression but not between component directions, the resultant force dependent component of yield criterion disappears and the Hill yield criterion (which describes orthotropic yield) is recovered.

5.3. Hill's criterion

Under transverse shear stress, Hill's criterion theory predicts yielding would initiate when the magnitudes of the stresses reach the following condition

$$\left(\frac{\sigma_1}{X}\right)^2+\left(\frac{\sigma_2}{Y}\right)^2+\left(\frac{\sigma_3}{Z}\right)^2-\left(\frac{1}{X^2}+\frac{1}{Y^2}-\frac{1}{Z^2}\right)\sigma_1\sigma_2-\left(\frac{1}{X^2}+\frac{1}{Y^2}-\frac{1}{Z^2}\right)\sigma_1\sigma_3$$
$$-\left(\frac{1}{X^2}+\frac{1}{Y^2}-\frac{1}{Z^2}\right)\sigma_2\sigma_3+\left(\frac{\tau_{12}}{S_{12}}\right)^2+\left(\frac{\tau_{13}}{S_{13}}\right)^2+\left(\frac{\tau_{23}}{S_{23}}\right)^2=1, \qquad (10)$$

where X, Y, Z are the yield strengths under uniaxial loading in each of the directions of material symmetry, and S_{12} is the in-plane shearing yield, while S_{13} and S_{23} are the transverse shearing yields. Both the tensile and compressive yild stresses may strain harden as functions of the equivalent plastic strain.

6. RESULTS AND DISCUSSION

Detailed discussion of the crashworthiness parameters is presented in the preceding sections. These are the crushing mechanism, crashworthiness parameters, failure modes, and the effects of design parameters on crashworthiness performance of FWL compound curved system subject to axial and lateral load conditions independently.

6.1. Crushing mechanism

Little data are available on the crushing mechanism of axially and laterally loaded filament wound laminated composite curved compound system. Such data are needed to understand failure mechanism modes, for verification of computational and design models.

6.1.1. Axial crushing. Typical load–displacement curves for the axially and laterally loaded FWL compound systems are shown in Figs 3 and 4. Load–displacement curves and deformation histories of ACSEM are plotted in Fig. 5. It can

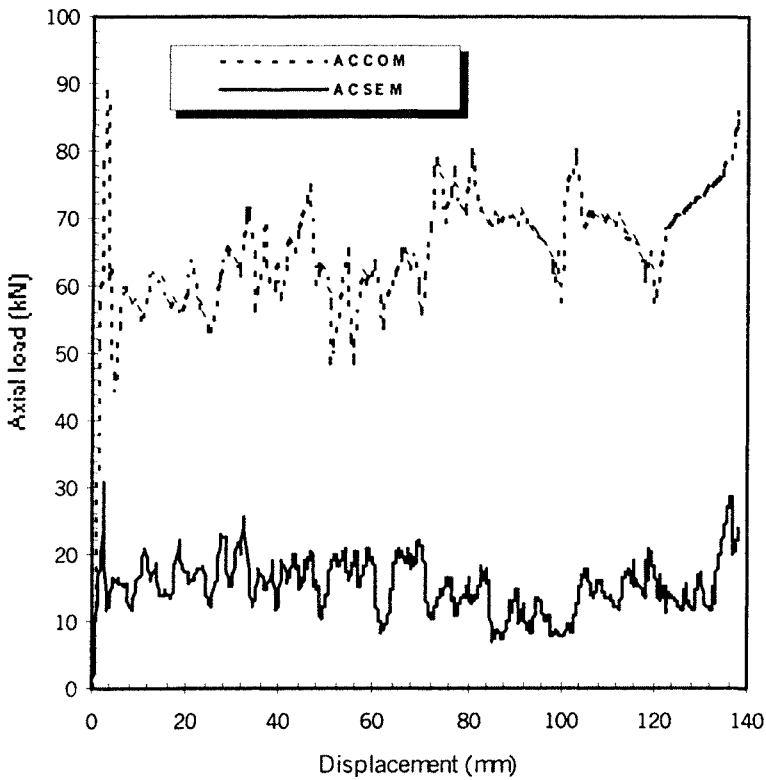

Figure 3. Load–displacement curves for FWL complete and semi-circular curved compound systems under axial compressive load.

be seen that the load–displacement curves have four sections. The first section describes the pre-crush stage (Fig. 5a), where the load increases to 87.9 kN and 31.0 kN for the ACCOM and ACSEM, respectively. The second section shows the failure initiation crush stage, where initial failure occurs at peak crush loads; at this instant the laminate stiffness at crush zone becomes evident and that results in a catastrophic drop in system load carrying capacity (see Fig. 5b). An abrupt large drop in load-carrying capacity is related to the fragmented and splayed zones. The magnitude of the load drops depends on the cross-sectional area over which the crack propagates as well as the failure mode. In the third section (Fig. 5c) the load–displacement curves become strongly non-linear beyond the initial failure point. In the non-linear range the axially loaded FWL c ompound systems exhibit unstable behaviour and fragmentation and spallation of the system wall takes place due to the transverse shear cracking and fragments are forced to the inside and outside of the system walls. After the crush zone initially had failed, it still had considerable strength and stiffness to continue its participation in carrying the total forces on the axially loaded FWL compound systems, but obviously at a reduced capacity. A rising load is a result of the reloading of the broken fibres and the regaining of the stable geometry by the crush interface. The shape of

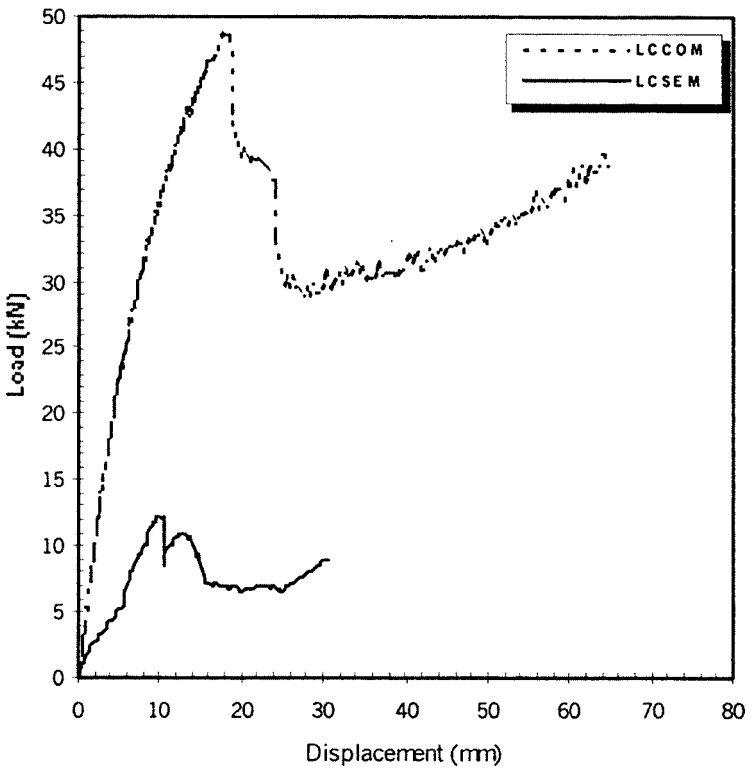

Figure 4. Load–displacement curves for FWL complete and semi-circular curved compound systems under lateral compressive load.

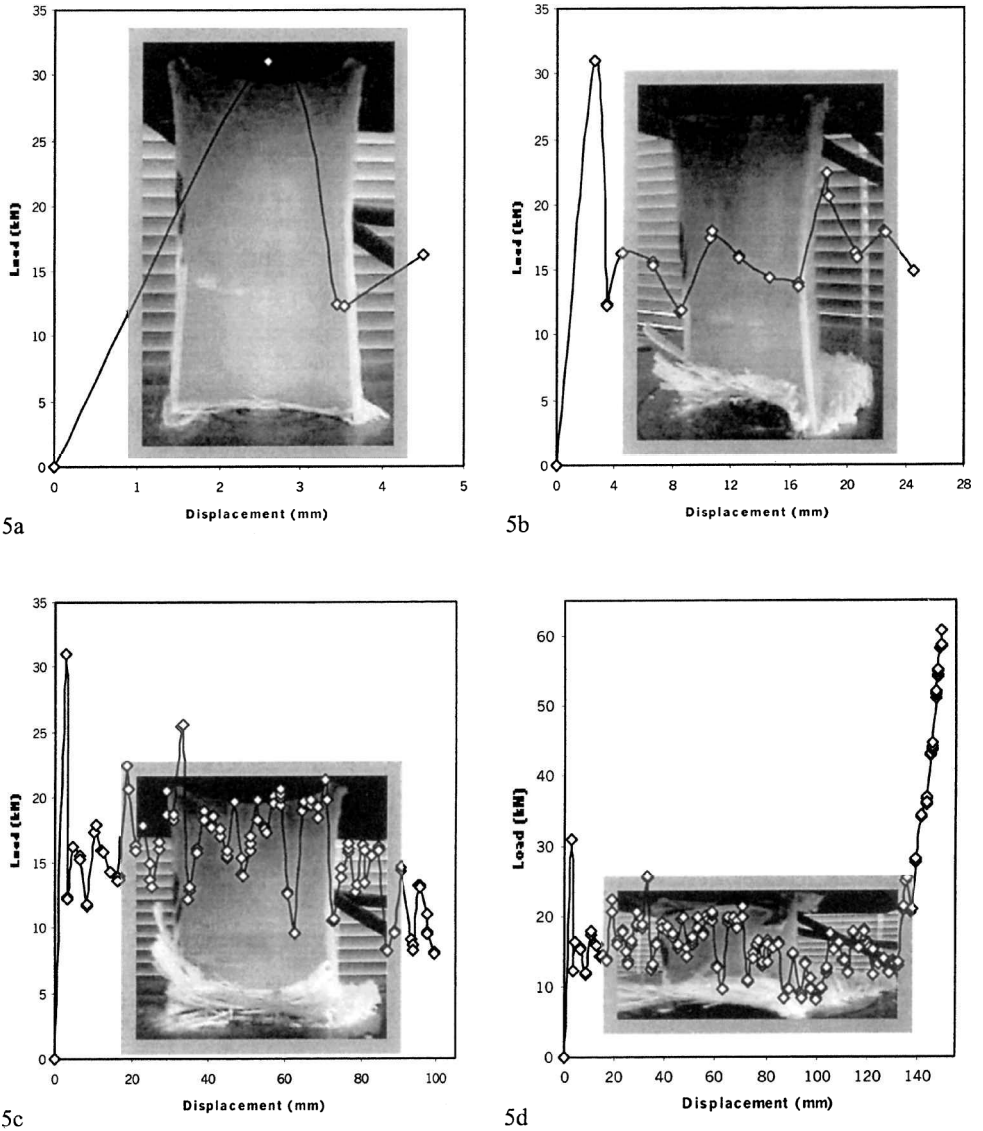

Figure 5. Load–displacement curves and deformation history for axially loaded semi-circular curved compound system.

the load–displacement curve in the post-crush stage is dominated by the energy absorbing capacity of the member up to the full crush. Figure 5d represents the fourth section, and presents the maximum compression possible in excess of testing machine stroke.

6.1.2. Lateral crushing. The instabilities are one of the more critical problems in using fibre composites for crash energy management. Instability is a state in

which the structure capacity for resistance to additional load is exhausted and continued deformation results in a decrease in load-carrying capacity. Unstable crash behaviour during collision is normally avoided by ensuring that the crushing of the loaded end occurs at load levels considerably lower than those required to cause the rest of the structure to fail. It is believed that to stabilise the crushing mechanism, the FWL curved compound system should be loaded laterally. Accordingly, typical load–displacement relations for the FWL curved compound systems under quasi-static lateral compressive load are shown in Fig. 4. Load–displacement curves and deformation histories of LCSEM are shown in Fig. 6. Dissimilar to the axially loaded FWL curved compound systems, the laterally loaded FWL curved compound system strength increases during the early stages after initial crush failure, as shown in Figs 6a and 6b. The occurrence of delamination at the bottom ends of the FWL curved compound system tends to weaken the load carrying capacity of the laterally loaded FWL curved compound system. Accordingly the load magnitude drops, as shown in Fig. 6c. Two energy absorption mechanisms related to friction were observed between the innermost surfaces of laterally loaded composite curved system specimens and the bottom plate; as the load increases the contact surfaces slide along the bottom plate. Moreover, another friction-related energy absorption mechanism was also observed due to the relative motion between adjacent layers that slide against each other. Accordingly the factional energy increases to slip a fibre along the fibre–matrix interface, as shown clearly in Fig. 6d. As the load increases, the LCSEM experiences transverse shear crack due to the tension state at the top layers and the compression state at the bottom and middle layers as the formation of longitudinal and transverse cracks in the system destroys its axial symmetry.

6.2. Failure modes

Under axial and lateral compressive loads, FWL compound systems crushed in a number of ways depending on the loading conditions. Two distinct crushing failure modes were observed during the quasi-static axial crushing test of the complete and semi-circular curved composite compound system. These modes can be identified and classified as follows.

6.2.1. Mode I. In this failure mode, the circumferential shear cracking initiates the failure mechanism at the loaded top end of the axially loaded complete and semi-circular curved composite compound system, which split the system crush zone wall circumferentially. This failure mechanism leads to a sharp catastrophic drop in load-carrying capacity. This abrupt loss in load-carrying capacity was due to an increase in the number of broken fibres at the loaded ends, which resulted in a low crush load at post-crush stage, as shown in Figs 3 and 5, as well as a lower energy mode with immediate reduction in crush force efficiency of the system.

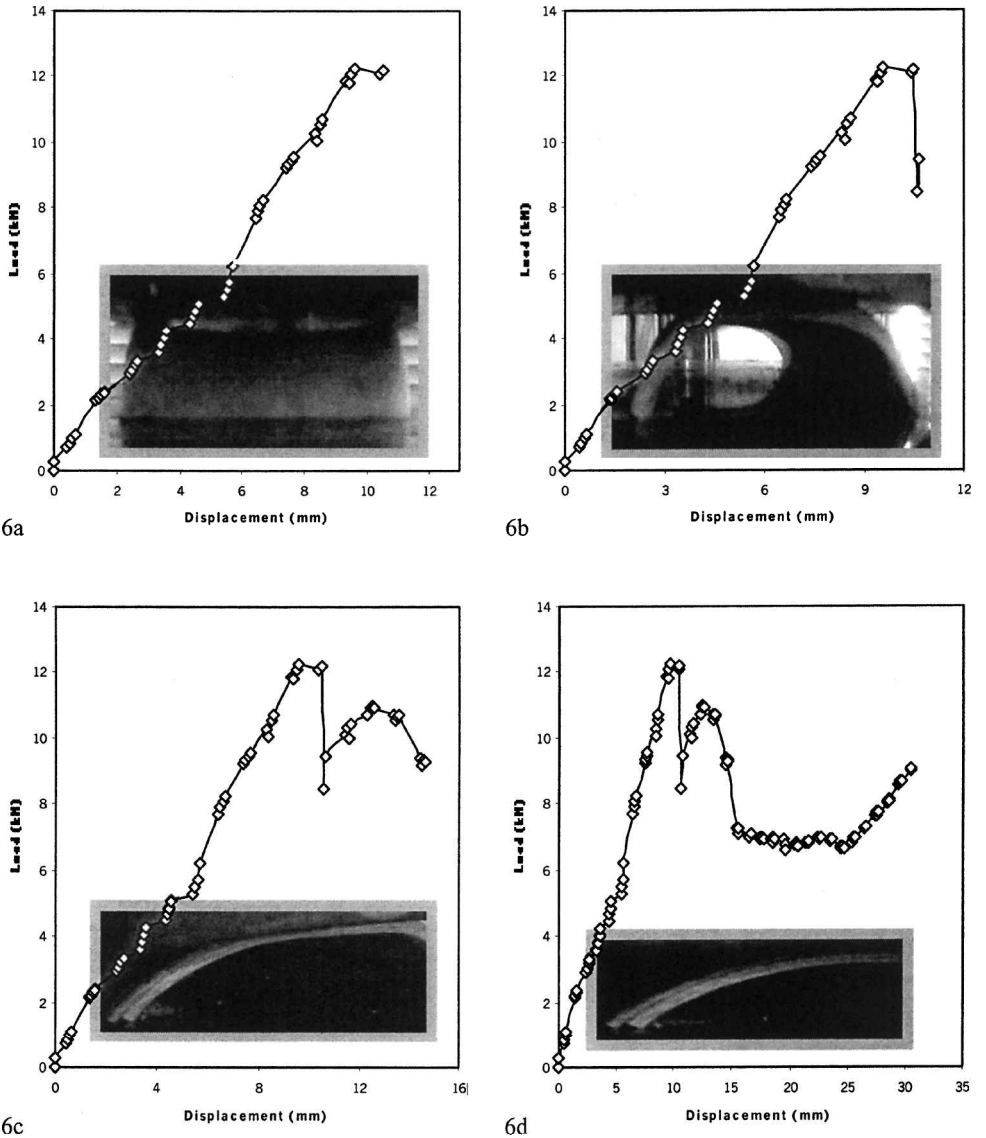

Figure 6. Load–displacement curves and deformation history for laterally loaded semi-circular curved compound system.

6.2.2. Mode II. This failure mode is associated with a stable failure mode that has been achieved by changing the load condition. When applying the lateral compressive load, the stresses at the loaded area are very high compared with stresses in the rest of the system: bending initiates in the loaded area and eventually a stable crush failure mode is generated, as shown in Figs 4 and 6. The crush force efficiency as well as stroke efficiency are observed to be larger than those measured for axially loaded FWL compound systems, i.e. mode I.

Table 1.
Measured and predicted crashworthiness parameters for the FWL complete and semi-circular curved compound system

SP. ID	P_i (kN)		P_m (kN)		*CFE* (%)		E_s (kJ/kg)		E_v (kJ/m^3)	
	EXP	FE	EXP	FE	EXP	FE	EXP	FE	EXP	FE
ACCOM	87.9	105.0	66.2	69.4	87.8	65.7	73.0	66.1	4701.9	4229.0
LCCOM	48.4	57.4	35.0	51.1	56.2	48.3	64.3	88.9	1890.1	3110.9
ACSEM	30.9	37.8	17.4	17.6	64.0	64.9	29.4	47.1	4139.6	4175.2
LCSEM	10.9	15.4	7.2	10.2	65.9	37.5	26.7	65.9	1717.7	2415.6

6.3. Crashworthiness parameters

It is of primary interest to ascertain the crashworthiness performances of FWL complete and semi-circular curved compound system specimens. Accordingly, the crashworthiness parameters of the axially and laterally loaded systems are given in Table 1. To adequately design an energy absorber device, it is necessary to determine the instantaneous crush failure loads relative to the initial crush failure load. Accordingly, a non-dimensional plot that provides such information is presented in Fig. 7a, b, where the instantaneous crush force efficiency is plotted against the stroke force efficiency. From this figure, it can be seen that the ACCOM displayed approximately 23% higher specific energy than LCCOM. In contrast the crush force efficiency of LCCOM seems to be higher than that of ACCOM. These are direct results of the load condition.

6.4. Crush simulation and experimental correlation

6.4.1. Simulation results for axially loaded system. The LUSAS predicted load–displacement curves for the axially loaded curved compound system are correlated with the experimental results in Figs 8b and 9b. In general, the simulation predicts the overall crush behaviour and magnitude of crush loads very well. On the other hand, the initial failure crush loads predicted are 105 and 38 kN, respectively, for ACCOM and ACSEM, which are 19% for ACCOM and 20% for ACSEM higher than experimental values.

6.4.2. Simulation results for laterally loaded system. In Figs 8a and 9a, the predicted load–displacement curves for the axially and laterally loaded FWL curved compound systems are correlated with the experimental one. However, the predicted initial failure crush loads were found to be 57 and 15 kN for the LCCOM and LCSEM, respectively. The plots indicate that the simulation is dissipating or removing energy at a faster rate than in the experiment, causing the model to stop sooner than the actual test. For example, at any displacement, the instant load of the experimental response is lower than that of the simulated response.

In Figs 5 and 6, the deformed shapes of the laterally and axially loaded FWL curved compound systems are shown in comparison to the deformed shape gener-

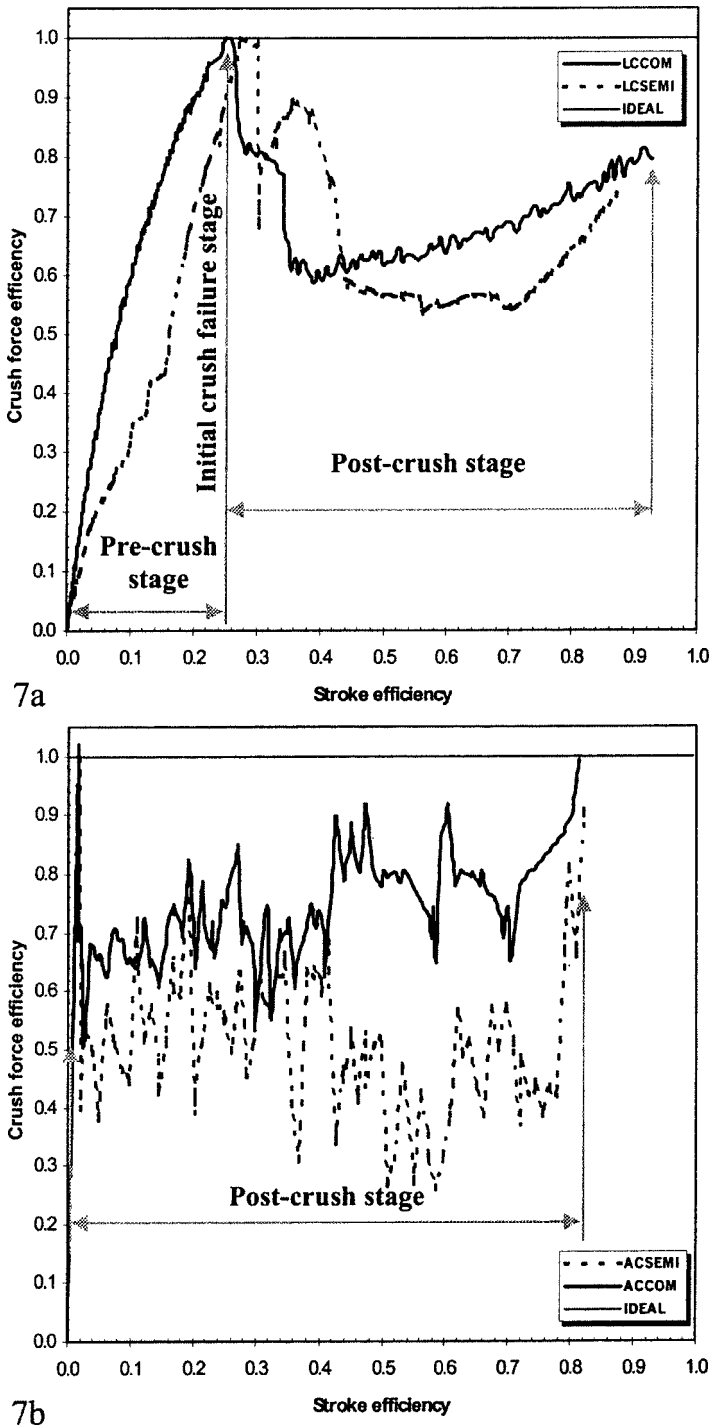

Figure 7. The normalized load–displacement curves for FWL complete and semi-circular curved compound system under lateral and axial compressive load.

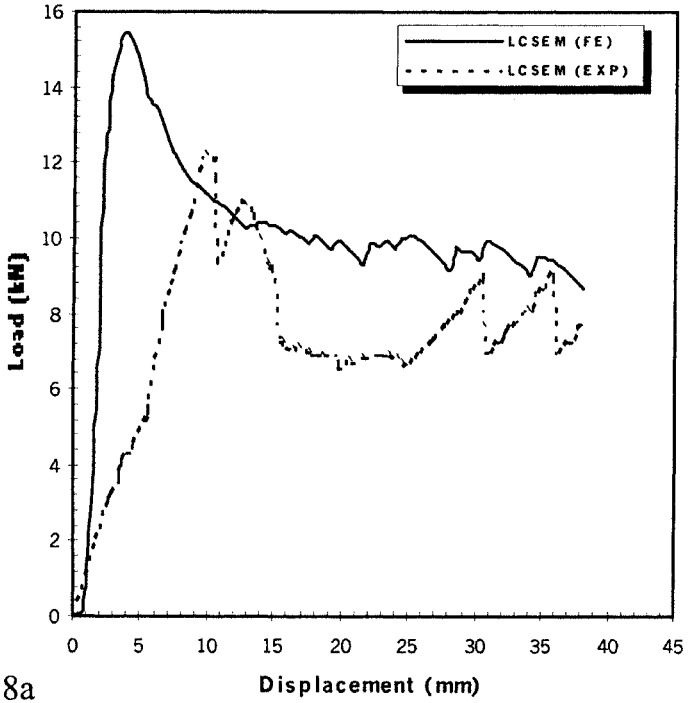

8a

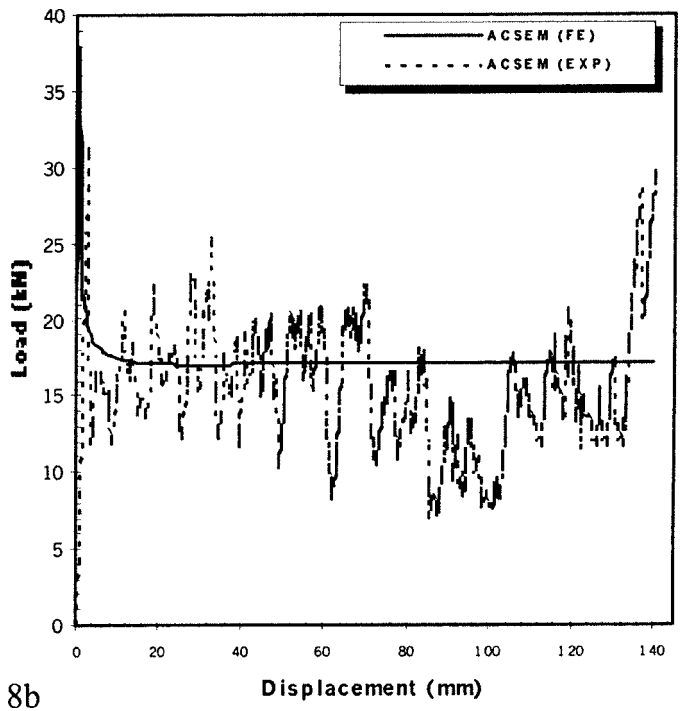

8b

Figure 8. The normalized load–displacement curves for FWL semi-circular curved compound system under lateral and axial compressive load.

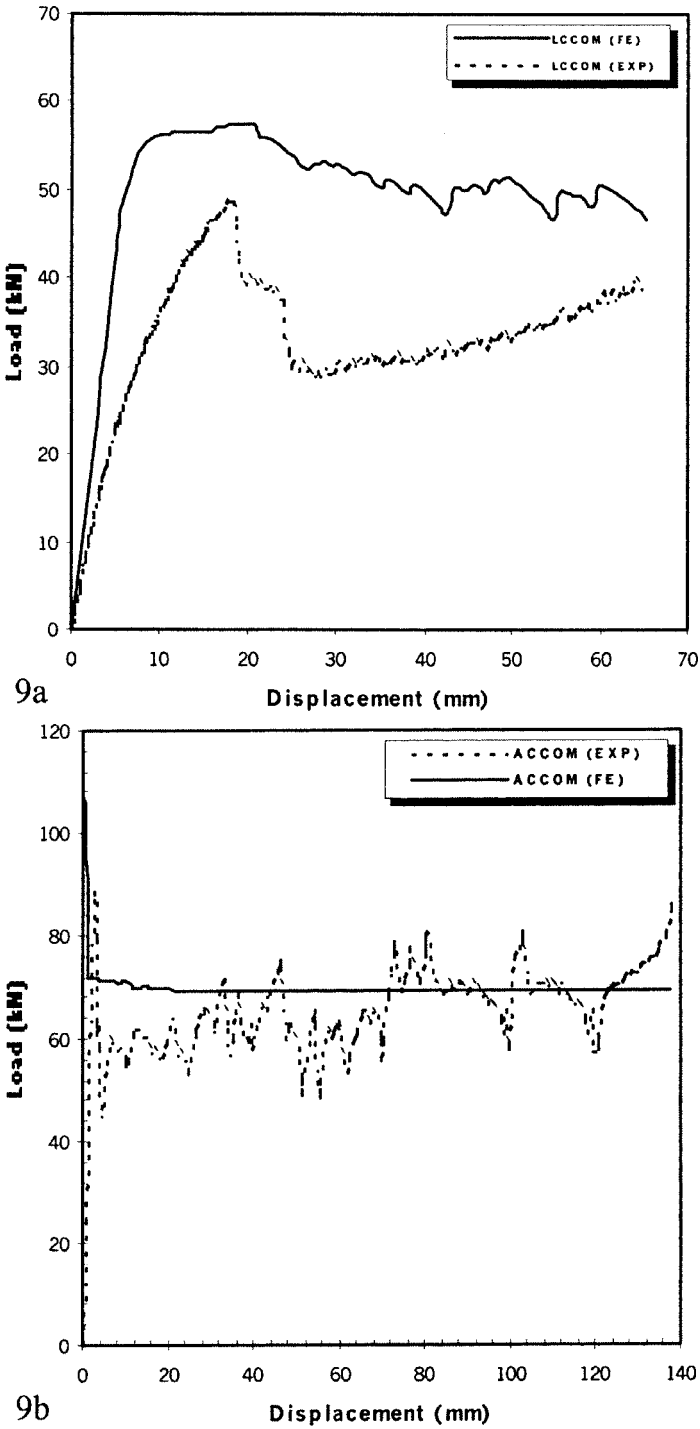

Figure 9. The normalized load–displacement curves for complete circular curved compound system under lateral and axial compressive load.

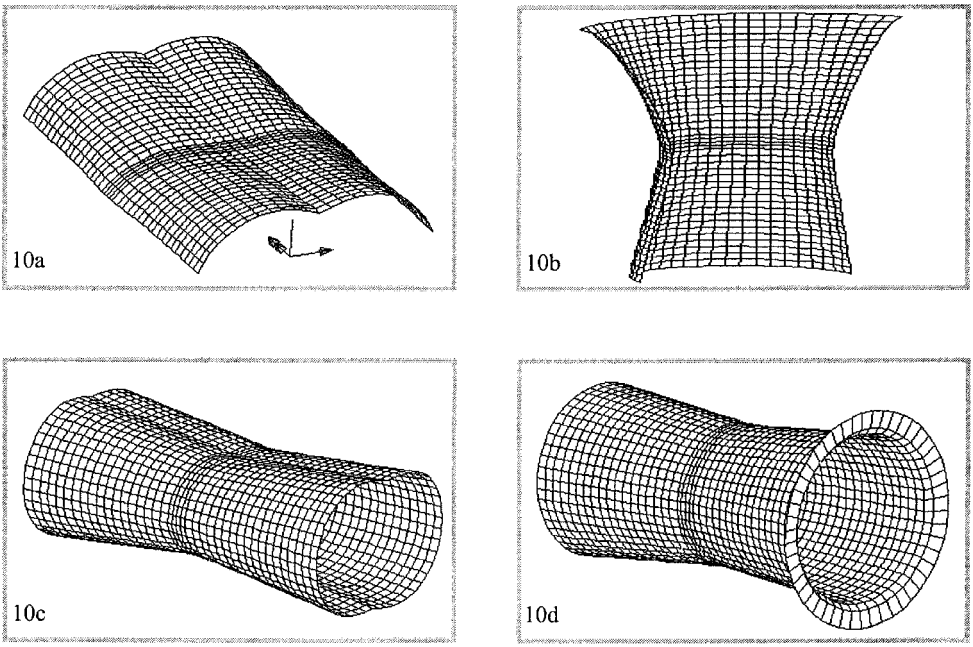

Figure 10. Deformed shape of laterally and axially loaded FWL complete and semi-circular curved compound systems at post-crush stage. 10a. LCSEM; 10b. ACSEM; 10c. LCCOM; 10d. ACCOM.

ated by the finite element model at post-crush stage as shown in Fig. 10. It could be seen that, similar to the experimental observation, the failure in the finite element model is initiated and started on the stress concentration regions. Moreover, effective stresses along the shell generator are presented in Fig. 11. Simulation provides in-plane shear stress distributions in material directions at the outer, middle and bottom layers, as shown in Fig. 12. Local stress was found to be concentrated at the junctions between the cylindrical and conical parts as well as the edges of the systems. It could also be seen from this figure that the in-plane shear stresses are highly non-uniform along shell generator.

6.4.3. Modelling inaccuracies. The divergences between the simulation and the experimental results may be attributed to the imprecise modelling of the FWL compound curved systems. The glass/epoxy material properties used were obtained from tensile tests on coupons. Consequently the material properties represent the tensile response and failure of the material only. During the initial crushing failure stage, the LCSEM and LCCOM systems were subjected to more complex loading scenarios, including the bending shear, which later caused the delamination at the edges of the LCSEM. In addition the primary reason for the differences between the simulation and the experiments is the complexity of failure modes that occur during the post-crush stages, which are absent from Hill's criterion. Moreover, the simulation model did not include the effect of imperfection, which greatly affects

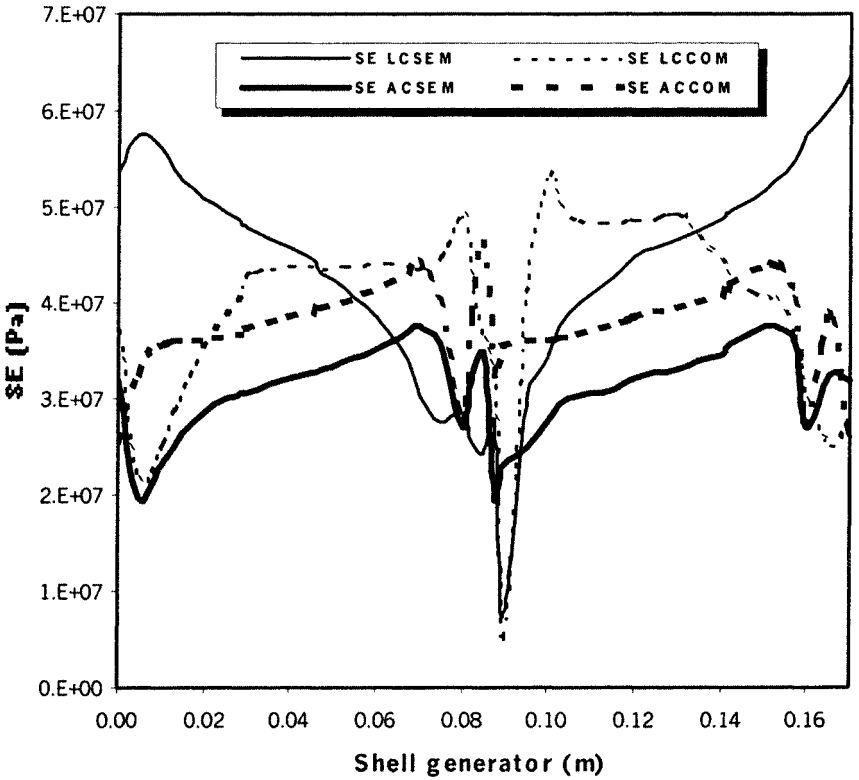

Figure 11. Effective stress for FWL curved compound system at post-crush stage.

the load-carrying capacity of any structure. In the finite element analysis, the work done due to friction between the shell surface and the platens is not considered. Overall, the simulation-developed model predicts the axial average failure crush loads of 66.2 and 17.4 kN while experiments measured average crush loads of 69.4 and 19.6 kN for ACCOM and ACSEM. The lateral average failure crush loads were 51.1 and 10.2 kN for LCCOM and LCSEM, which are 46% for LCCOM and 41% for LCSEM higher than experimental values.

Justification for the over-simulation prediction values of load–displacement behaviour during the post-crush stage for the axially and laterally curved compound system is that the delamination and debonding failure modes are not incorporated in Hill's criterion.

7. CONCLUSIONS

In this study, the crushing behaviour of FWL curved compound systems have been studied experimentally and numerically under axial and lateral loads. In all cases, the predictions of the simulations agreed reasonably well with the experimental evidence. Based upon the test results the following conclusions can be drawn:

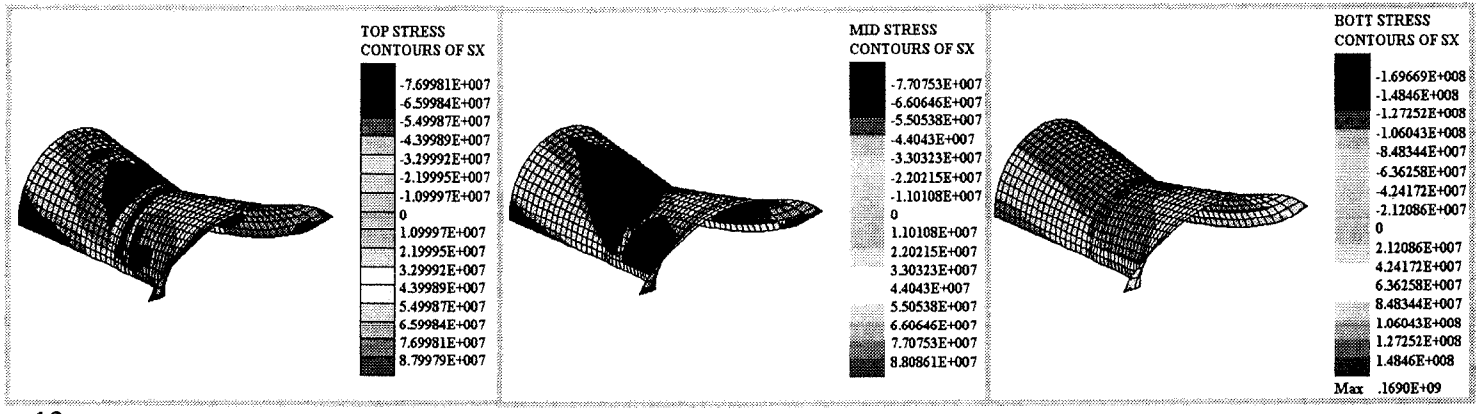

12a

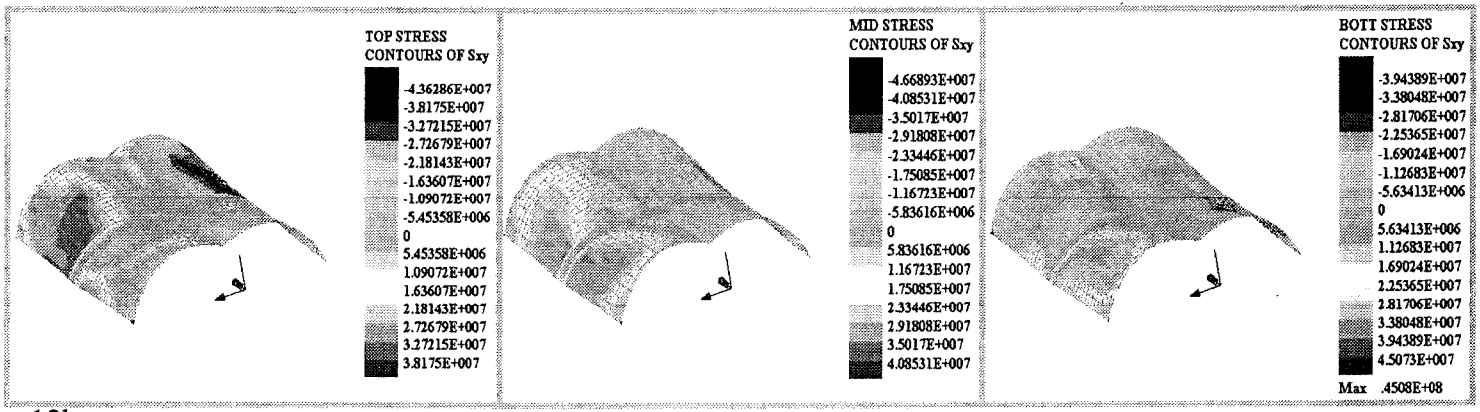

12b

Figure 12. In-plane shear stress of axially and laterally loaded complete and semi-circular curved composite compound system contour during post-crush stage. 12a. LCSEM; 12b. ACSEM; 12c. LCCOM; 12d. ACCOM.

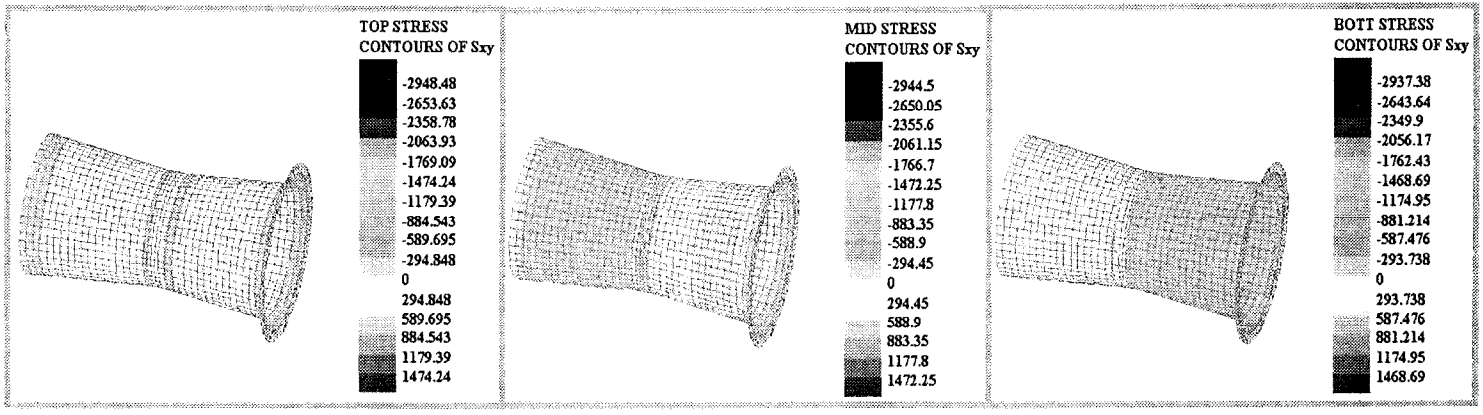

12c

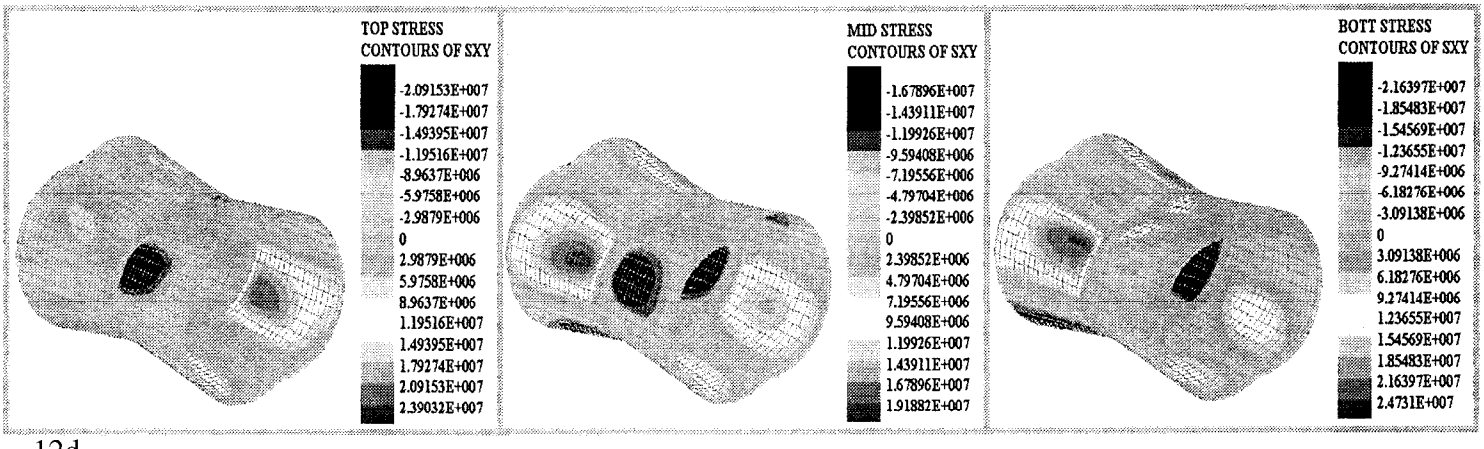

12d

Figure 12. (Continued).

1. The laterally loaded composite curved system specimens show stable crush behaviour and their walls start to buckle and delaminate at low stresses allowing for extensive compression with an adequate deceleration path.
2. Although the axially loaded composite curved system specimens were stronger and stiffer than the laterally loaded one, their crush behaviour is often unstable, with energy absorption increasing and decreasing randomly.
3. A change in load condition affects the crush loads significantly.
4. Friction force between the innermost surface of laterally loaded composite curved system specimens and the bottom plate is substantially affects the post-crush stage.
5. A stable post-crushing stage leads to high crashworthiness performance.
6. High initial failure crush load leads to catastrophic failure mode as well as unstable post-crush stage.
7. An axially loaded curved compound system seems to be more rigid than the laterally loaded types.

Acknowledgements

The authors wish to thank Universiti Putra Malaysia for the financial support for this research programme.

REFERENCES

1. S. G. Thomas, S. R. Reid and W. Johnson, Large deformation of thin walled circular tubes under transverse loading-I, *Int. J. Mech. Sci.* **18**, 325–333 (1976).
2. W. Johnson and S. R. Reid, Metallic energy dissipating systems, *Appl. Mech. Rev.* **31**, 277–288 (1978).
3. V. Tvergaard, On the transition from a diamond mode to an axisymmetric mode of collapse in cylindrical shells, *Int. J. Solids Structures* **19** (10), 845–856 (1983).
4. N. Jones, *Structural Crashworthiness.* Butterworths, London (1983).
5. S. R. Reid, Plastic deformation mechanism in axially compressed metal tubes used as impact energy absorbers, *Int. J. Mech. Sci.* **35**, 1035–1052 (1993).
6. T. Y. Reddy and S. T. S. Al-Hassani, Axial crushing of wood filled square metal tubes, *Int. J. Mech. Sci.* **35**, 231–246 (1993).
7. L. Wu and J. F. Carney, Experimental analysis of collapse behaviour of braced elliptical tubes under lateral compression, *Int. J. Mech. Sci.* **40** (8), 761–777 (1998).
8. M. D. White and N. Jones, Experimental quasi-static axial crushing of top hat and double-hat thin-walled sections, *Int. J. Mech. Sci.* **41**, 179–208 (1999).
9. A. Hanssen, G. M. Langseth and O. S. Hopperstad, Optimum design for energy absorption of square aluminium columns with aluminium foam filler, *Int. J. Mech. Sci.* **43**, 153–176 (2001).
10. D. Hull, Energy absorption of composite materials under crash conditions, *Progress in Science and Engineering of Composites* (1982).
11. G. L. Farely, Energy absorption of composite materials, *J. Compos. Mate.* **20**, 322–334 (1986).
12. C. A. Meyers and M. W. Hyer, Response of elliptical composite cylinders to axial compression loading, *Mech. Compos. Mater. Struct.* **6** (2), 169–194 (1999).

13. D. Hull, A unified approach to progressive crushing of fibre-reinforced composite tubes, *Compos. Sci. Technol.* **35** (3/4), 231–246 (1993).
14. G. D. Mamalis, E. Manolakos, G. A. Demosthenous and M. B. Ioannidis, Analytical modelling of the static and dynamic axial collapse of thin-walled fibreglass composite conical, *Int. J. Impact Engng.* **19** (5–6), 477–492 (1997).
15. J. C. Riddick and M. W. Hyer, The responses of segmented-stiffness composite cylinder to axial end shortening, *Composite Structures* **40** (2), 103–114 (1998).
16. P. Knoedel, Cylinder-cone-cylinder intersection under axial compression, in: *International Colloquium on Buckling of Shell Structures on Land, in the Sea and in the Air*, Lyon, France, 17–19 September, pp. 296–303. Elsevier (1991).
17. R. Greiner and R. Ofner, Elastic plastic buckling at cone-cylinder junctions of silos, in: *International Colloquium on Buckling of Shell Structures on Land, in the Sea and in the Air*, Lyon, France, 17–19 September, pp. 296–303. Elsevier (1991).
18. C. T. F. Ross, Design of dome ends to withstand uniform external pressure, *J. Ship Res.* **31**, 139–143 (1987).
19. E. Mahdi, B. B. Sahari, A. M. S. Hamouda and Y. A. Khalid, An experimental investigation into crushing behaviour of filament wound laminated cone-cone intersection composite shell, *Composite Structures* **51** (3), 211–219 (2001).
20. E. Mahdi, Crushing behaviour of laminated circular cylindrical, conical and compound composite shells of revolutions, Doctorate thesis, Universiti Putra Malaysia (2000).
21. A. A. A. Alghamdi, Collapsible impact energy absorbers: an overview, *Thin-Walled Structures* **39** (2), 189–213 (2001).
22. N. K. Gupta and H. Abbas, Lateral collapse of composite cylindrical tubes, *Int. J. Impact Engng* **24**, 329–346 (2000).
23. S. Ramakrishna and H. Hamada, Energy absorption characteristics of crash worthy structural composite materials, *Key Engineering Materials* **141–143**, 585–620 (1998).
24. K. Takahashi, K. Ban and T. Sakai, Analysis of the effect of fibre orientation distribution in elastic reinforcement theory (in Japanese), *J. Society of Materials Science, Japan (Zairyo)* **26** 1232–1243 (1977).
25. LUSAS/standard User's Manual, LUSAS theory manual, version 13.1.